

Performance of an Optical Seismometer from 1 μ Hz to 10 Hz

by Jonathan Berger, Peter Davis, Rudolf Widmer-Schmidrig, and Mark Zumberge

Abstract We compare the performance of four different instruments that measure the vertical component of motion of an inertial mass—an STS1 seismometer, an STS2 seismometer, a superconducting gravity meter, and an optical seismometer—operating inside the mine at the Black Forest Observatory near Schiltach in southwest Germany. Simultaneous, collocated operation of these sensors offers an opportunity to test the calibration, response, and performance of each instrument. We estimate noise floors from the tidal bands to 10 Hz. We note small nonlinearities in the suspension of the STS1, which are normally suppressed by analog signal processing and feedback or, in the optical version, by digital signal processing alone. The results demonstrate that the optical seismometer utilizing an STS1 suspension can provide observatory-quality data over a bandwidth from tidal frequencies to at least 10 Hz and over a large dynamic range.

Introduction

Seismic instrumentation with high linearity and high dynamic range is critical for many seismological applications, such as locating and characterizing earthquakes and other seismic sources, studying crustal structure, and probing the deep interior of the Earth. The Global Seismic Network (GSN) strives to operate the best seismometers at scores of stations around the world. It is very important to understand the advantages and limitations of different sensors so that the capabilities of the GSN can be optimized. We have analyzed records from four quite different sensors, all operating at the same location, to investigate their relative performances. We are interested in their dynamic range, bandwidth, linearity, and calibration precision and stability. The dynamic range depends on the instrument's clip level and its resolution (noise level). The bandwidth is a measure of the minimum and maximum frequency over which observations can be made. The linearity is a measure of the ability to represent the instrument's output as a linear operator on the ground motion. Finally, the calibration is a determination of the mathematical function that relates the ground motion to the instrument's output across its operational bandwidth.

Seismometers can be calibrated in many ways. Usually, there are two key aspects to the calibration: the relative variation in the instrument response with frequency, and the overall gain of the seismometer. This is a scale factor that relates physical units of ground motion to the instrument's output. It is, of course, important to establish these characteristics precisely. The sensors described here are each calibrated in different ways and have different frequency responses, affording the opportunity to test the calibrations against one another.

In this study, we compare a number of instruments, all installed in the tunnels of the Black Forest Observatory (BFO; [Data and Resources](#)). There are two conventional seismometers (STS1 and STS2), a superconducting gravimeter

(SG), and an optical seismometer (iSTS1); details are given in Table 1. The observatory is located in the middle of the Black Forest in southern Germany far from potential sources of anthropogenic noise. Instruments are deployed in a former silver mine, which was excavated horizontally into a hillside of competent granite reaching depths of up to 170 m below the surface and a maximum distance of 700 m from the entrance (Fig. 1). The sites within the mine are very stable thermally. Two airlocks provide additional protection against rapid air-pressure variations and contribute to thermal stability. Both the SG and the iSTS1 are installed between the inner and outer airlock, and the STS1 and the STS2 are installed behind the inner airlock, affording them slightly better immunity to environmental noise.

The STS1 and the STS2 have had, by far, the most time (decades) to stabilize and are located in a marginally better environment (deeper in the mine and behind a second airlock). Although the mechanical part of the iSTS1 is more than two decades old, the instrument was modified during the two-year period prior to its installation at BFO in 2010. The modifications, other than disconnection from its usual set of feedback electronics, included removal of one of the two main brass masses, machining it to accommodate the mounting of a cornercube retroreflector, and the addition of optics beneath the base for the interferometric tracking of the mass position. As part of this, the magnetic shield was omitted. The SG was installed in 2009.

We carry out the comparisons in three frequency bands: Earth tides, 1–100 μ Hz; normal modes, 0.2–1 mHz; and teleseismic, 0.01–10 Hz. The designers of the STS1 and STS2 aimed for optimum performance (i.e., high sensitivity and low noise) in the normal mode and teleseismic bands, whereas the inventors of the SG were more focused on its behavior at tidal and subtidal bands (e.g., the Chandler wobble

Table 1
Instruments Used in This Study

Instrument	Network	Details
STS-1Z (SN 28740)	Incorporated Research Institutions for Seismology/International Deployment of Accelerometers (IRIS/IDA)	Installed February 1993; 360 s force balance recorded on Mk7B and since 2011 on Q330 data logger.
STS2 (SN 19123)	German Regional Seismic Network (GRSN)	Installed in May 1992; 120 s force balance triaxial recorded on Q680 until October 2011 and thereafter on a Q330HR.
iSTS1 (modified optical)	n/a	Installed September 2010. Interferometric displacement sensor on STS-1Z suspension. Recorded on 16-bit digital signal processor (femtometer) with 30-bit dynamic range.
SG (OSG-056)	Global Geodynamics Project (GGP), IRIS/IDA	Installed September 2009. Dual sphere superconducting gravimeter recorded on a digital voltmeter and also on a Q330HR since October 2011.

at a 14-month period). Because of their design parameters, we omit the SG from the comparisons at high frequencies and we omit the STS2 from comparisons at tidal frequencies. The design of the optical seismometer is an attempt to cover the entire signal spectrum from DC (zero frequency) to 100 Hz.

The STS1 Seismometer

The STS1 seismometer has been the mainstay of long-period seismology for the past two decades. In particular, it is the primary sensor of the GSN. The seismometer employs a leaf-spring suspension with a Linear Variable Differential Transformer displacement transducer and electromagnetic force feedback (Wielandt and Streckeisen, 1982). The mass displacement signal is processed by analog electronics to produce a feedback signal that forces the mass to remain stationary with respect to its housing. The sensor’s processed output is an analog voltage proportional to ground velocity in the bandwidth from 2.78 mHz (360 s) to about 10 Hz (Fels and Berger, 1994). One of the effects of using feedback is that the sensitivity must be reduced to avoid saturation of the feedback electronics at periods longer than 360 s due to thermal effects and suspension drift and at frequencies above about 10 Hz to achieve stability. The calibration of the instrument used in this research was done in January 2011. The frequency-dependent relative calibration of the STS1 was done by injecting both a sweep and a random binary telegraph signal into the calibration coil and modeling the response of the seismometer. The absolute gain was estimated by comparison with a collocated STS2 for which absolute sensitivity had previously been determined on a calibration table (Wielandt, 2012). The particular STS1 we examine in this study has been operational in a very stable environment for over 20 years. Further, it consistently records among the lowest noise levels in the entire GSN (Berger *et al.*, 2004).

The STS2 Seismometer

The STS2 is a force-balance seismometer with three identical inertial masses in a triaxial arrangement, each oriented at about 55° to the vertical. Output is proportional to

ground velocity over the band from 8.33 mHz (120 s) to about 30 Hz. The STS2 at BFO is operated as part of the German Regional Seismic Network. The calibration of the STS2 seismometer in this case is supplied by the manufacturer.

The Superconducting Gravimeter

In an SG (manufactured by GWR Instruments, Inc.), the proof mass normally suspended on a mechanical spring of a classical seismometer is replaced by a superconducting sphere, which is levitated in the persistent magnetic field from the current in superconducting coils. During installation, the magnetic field is adjusted to levitate the sphere and provide a small gradient so as to produce a large displacement of the mass for a small change in ground acceleration or, equivalently, a small change in gravity (Goodkind, 1999). A pair of hemispherical capacitor plates provides the means of mass displacement sensing, and a normal coil provides force feedback to keep the sphere centered between the capacitor plates. The current in this coil is proportional to ground acceleration, and this is the recorded signal. At BFO, the instrument is housed in a stainless steel chamber within a Dewar, which includes a closed-cycle refrigeration unit to keep the superconducting elements at the required temperature of 4 K. Absolute calibration for the SG was determined by comparison with a nearby absolute gravimeter (Widmer-Schmidrig *et al.*, 2012), which is different from older methods (e.g., Van Camp *et al.*, 2000). Because the signal sensed by these instruments is dominated by the diurnal and semidiurnal tides, such experiments yield the response at tidal frequencies, at which the SG output is strictly proportional to acceleration (the full response was determined by Heck, 2014). The SG was installed in 2009. Thus far, four calibration campaigns lasting between two and five days were conducted, and the DC gain was found to be stable to within 0.4%.

In this study, we use the data from the lower, heavier sphere (17.7 g), which is the less noisy of the two levitated spheres in the SG, and we limit our analyses of it to periods longer than 3 s because its design is optimized for low frequencies. This instrument has the lowest noise levels in the seismic

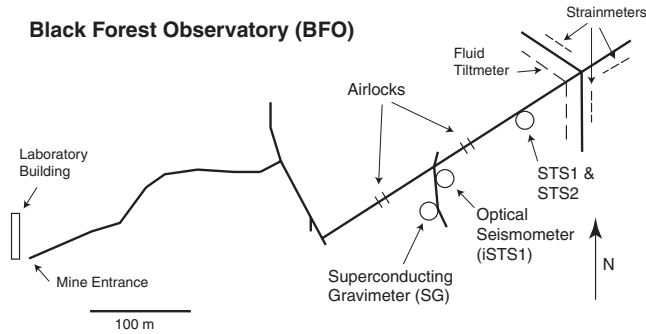


Figure 1. Schematic view of the mine showing the location of the instruments. The horizontal tunnel was excavated into granite basement and reaches a depth of 170 m below the surface.

and subseismic bands of any in the Global Geodynamics Project Network (Rosat and Hinderer, 2011).

The Optical Seismometer (iSTS1)

The essence of the optical seismometer (Zumberge *et al.*, 2010) is an interferometer that measures the motion of an inertial mass using laser light and optical fibers. In this particular instrument, we utilize the suspension of a modified vertical component STS1 (hence “iSTS1”) and eliminate all electronics associated with the normal position sensor, forcer, and feedback electronics. A free-space Michelson interferometer illuminated with a 1 mW laser is linked to the seismometer with optical fibers. Two 16-bit digitizers sample the interference fringe signals at 100,000 samples per second and digitally process them to produce a 400-samples-per-second record of both mass displacement (Zumberge *et al.*, 2004) and ground acceleration using the nonlinear differential equation

$$-G\ddot{z} = \ddot{x} + \frac{\omega_0}{Q}\dot{x} + \omega_0^2x + c_1x + c_2x^2, \quad (1)$$

in which z is the ground displacement, G is a unitless number related to the moment of inertia of the suspended mass compared to a point mass (Zumberge *et al.*, 2010), x is the mass displacement relative to the frame ($x = 0$ is the equilibrium position), ω_0 is the resonant frequency, and Q is the quality factor from the damping in the suspension. The last two terms in equation (1) include adjustable constants c_1 and c_2 to compensate for any suspension offset or nonlinearity that may occur for large mass displacements. (In this context, “larger” means of order 1 mm; this is rare—there have only been a few instances in which this has been encountered since our installation at BFO.) The maximum mass displacement is limited by mechanical issues to a few millimeters. The 100,000-samples-per-second rate limits the maximum mass velocity to 15 mm/s (Zumberge *et al.*, 2004). In terms of mass displacement, the dynamic range is at least 1×10^9 , equivalent to 30 bits. The instrument bandwidth extends from DC to about 100 Hz. The method by which the instrument is calibrated is described in the next section.

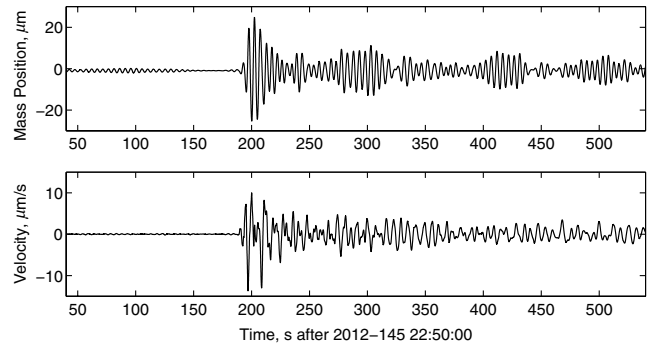


Figure 2. The raw mass displacement signal is dominated by the freely oscillating mass because the Q is high (22 for the optical seismometer, iSTS1) and the free period is close to the microseism peak. The upper plot is an example of the mass position following a disturbance from an earthquake (magnitude 6.2 in the Norwegian Sea). However, armed with the parameters that govern the suspension, the ground velocity is easily computed using equation (1); the result is shown in the lower trace, and it agrees with the record from a collocated conventional seismometer.

At seismic frequencies, we can infer ground acceleration from mass position via equation (1) when we know G , Q , and ω_0 (the next section describes how we obtain these). As an example, Figure 2 shows the actual mass position record produced by an earthquake and the ground velocity inferred from it.

Tidal Studies

Calibration of the iSTS1

Observations of Earth tides are routinely used as a method of calibrating vertical seismometers and gravimeters because the Earth tides produce narrowband signals, which can be accurately predicted (Davis and Berger, 2007). We made use of this to calibrate the optical seismometer after its installation in the mine.

From equation (1) for the optical seismometer, we see that for small mass displacements and at frequencies that are low compared with the resonant frequency, the mass position follows changes in gravity Δg :

$$\ddot{z} = \Delta g = -G^{-1}\omega_0^2x \quad \omega \ll \omega_0 \quad x \ll x_{\max}. \quad (2)$$

Therefore, the ratio of ground acceleration to mass displacement in the nonfeedback optical seismometer depends upon both mechanical elements of the seismometer construction, which should be constant for an undisturbed instrument, and the resonant frequency, which in principle may change with time.

The resonant frequency, however, is easy to estimate at any time by calculating the spectrum of the observed mass position and performing a least-squares fit of a section of the spectrum around the nominal resonant frequency to the theoretical response from equation (1) above. We can estimate the resonant frequency very well, easily to better than one part in

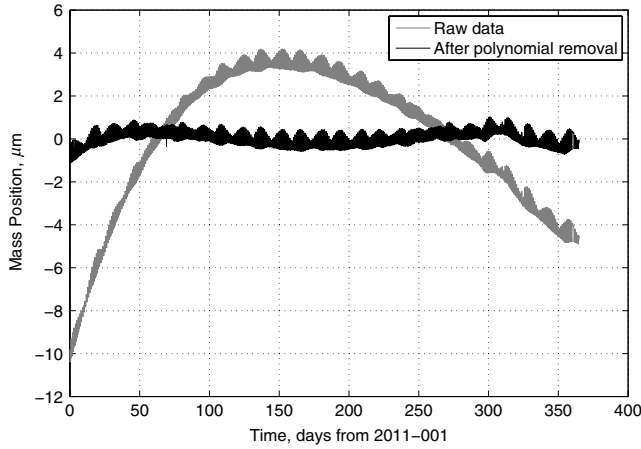


Figure 3. The gray trace is the iSTS1 mass position, low-pass filtered (with only an offset removed), and the black trace has had a third-order polynomial subtracted. At periods much longer than the spring suspension’s free period, mass position is proportional to gravity, so the gravity tidal signal is clearly resolved.

10^4 . Evaluation of Q is less critical and is done adequately with the same method. Both parameters seem quite stable on the undisturbed iSTS1; at BFO, the resonant frequency, $\omega_0 = 1.304 \text{ s}^{-1}$, has changed by less than 0.1% and the damping, given by $Q = 21.8$, by less than 1% over the period of a year.

To determine the factor G in equation (2), which depends solely on the mechanical geometry of the suspension, we make use of the fact that we can calculate very accurately the vertical ground acceleration at tidal frequencies, including the effects of ocean loading (Agnew, 1996). Treating this acceleration as the input signal, we then form the ratio of this to the observed mass displacement (i.e., the output signal) and determine G . For tidal signals, x is small; this allows us to assume that c_1 and c_2 are negligible.

For this tidal analysis, the first step is to remove the long-term drift in the mass displacement record by modeling it as a polynomial in time. We analyzed one year (2011) of edited iSTS1 data, downsampled to 1 sample per five minutes (Fig. 3). The editing consisted only of adjusting for spurious offsets and low-pass filtering for decimating the time series.

Next, we fit both the theoretical tide and the observations (with the long-term drift removed, i.e., the flattened trace in Fig. 3) to a series of sine waves at the tidal frequencies using a MATLAB tidal fitting toolbox (see [Data and Resources](#)). Because the amplitude of the tidal component M2 is both relatively large and well separated in frequency from other components, we use the ratio of observed to theoretical M2 amplitudes to estimate G . In addition to this analysis of the entire year, we also performed the same analysis using 50% overlapping, 73-day sections and taking the average of these values. Both methods gave the same result: $G = 0.722$, with a standard deviation from the averaged sections of 1%. Figure 4 shows the results. Other methods to determine the suspension’s relevant coefficients are given in [Zumberge et al., 2010](#).

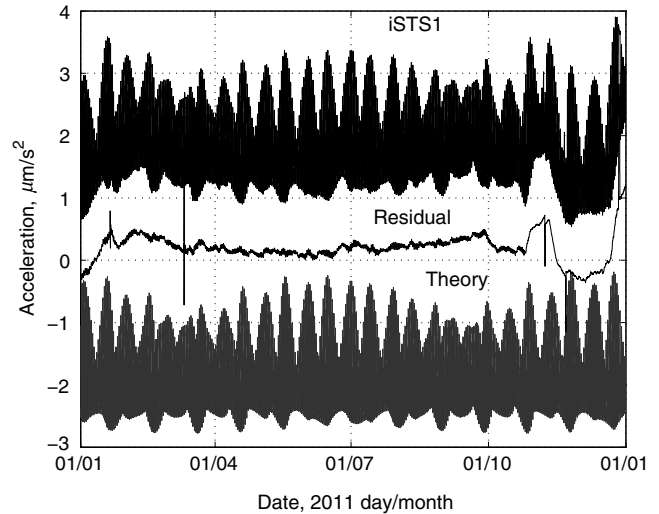


Figure 4. The upper trace is the calibrated ground acceleration from the iSTS1, smoothed in this instance with a fourth-order polynomial, and the lower trace is the theoretical tide used for the calibration. The middle trace is the difference.

Tidal Spectra

We examined a 65-day epoch from the STS1, the iSTS1, and the SG to compare how well each sensor recorded tidal signals. Figure 5 shows the tide residuals over this epoch for these instruments. For each sensor, we used the MATLAB toolbox mentioned above to fit tidal lines to the observed time series (top traces). We then constructed a theoretical time series (bottom traces) from the tidal coefficients obtained in that fit and subtracted these from the observed data to produce a time series of residuals (middle traces).

Each of these observed time series was scaled to an approximation of acceleration using a single sensitivity value appropriate for the frequency of the principal semidiurnal tidal component, M2. The sensitivity used to scale the iSTS1 series was obtained in the previous section. The sensitivity values for the STS1 ($4.2454 \times 10^{10} \text{ counts/m/s}^{-2}$) and the SG ($2.496 \times 10^6 \text{ volts/m/s}^{-2}$) were obtained from the Incorporated Research Institutions for Seismology Data Management Center’s (IRIS DMC) response database. The SG sensitivity is based on comparisons with an absolute gravity meter and the STS1 on comparison with a table-calibrated STS2. Because its response function at tidal periods is not flat, the STS1’s velocity output was deconvolved according to the known response to give the acceleration time series shown in Figure 5.

We also fit the theoretical tide and then examined the observed-to-theoretical ratios of the principal semidiurnal tidal component, M2. Ideally, these ratios would be 1.00, but in fact we get 1.005 for the iSTS1, 1.016 for the SG, and 0.986 for the STS1. (Of course, the M2 tide for the full year was used to determine the effective calibration constant of the iSTS1, so the agreement with the 65-day segment is to be expected.) Eliminating the calculation of the theoretical tide, we determine that the ratio of observed M2 tide on the iSTS1 is 0.989 times the observed M2 tide on the SG.

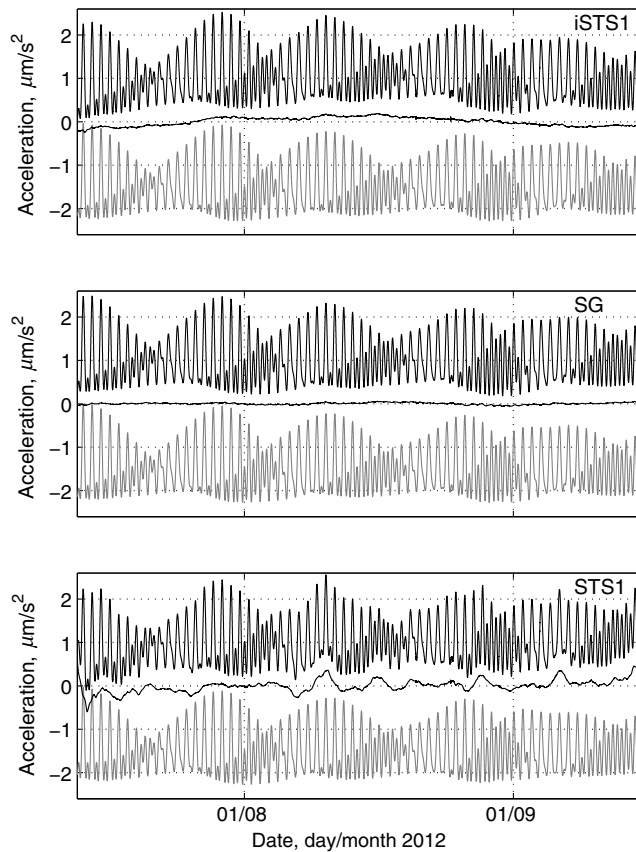


Figure 5. Observed tides (upper traces) and residuals after subtracting fitted tidal constituents (lower traces). For the iSTS1 and the superconducting gravimeter (SG), the task is straightforward because both have responses that are flat to acceleration from zero to seismic frequencies. For the STS1, we first converted its velocity output to acceleration using its known transfer function.

It is well known that the atmosphere exerts a gravitational attraction on the inertial mass of a seismometer. We can easily see this by examining the residuals after removal of the tides (Fig. 6). We have approximated this effect by subtracting from the observed ground acceleration $3.5 \times 10^{-11} \text{ m/s}^2/\text{Pa}$ (Widmer-Schmidrig, 2003) multiplied by the local barometric pressure signal.

After correcting for the barometric pressure effect, we estimate the spectra of the 65-day time series using a Hanning window and a bandwidth of $2.54 \times 10^{-7} \text{ Hz}$. The results are shown in Figure 7.

For frequencies below about $1 \times 10^{-4} \text{ Hz}$, the SG noise levels are lowest. There was significant improvement in the iSTS1 and SG noise level in this band after correcting for the pressure record. The improvement at 2 μHz was 10 dB for the iSTS1 and 12 dB for the SG. (We found no such improvement for the STS1.)

Higher Frequencies

For higher frequencies, we compared the observed noise on the BFO vertical instruments during an 88 hr epoch beginning on 28 March 2012 (Fig. 8). The third percentile of

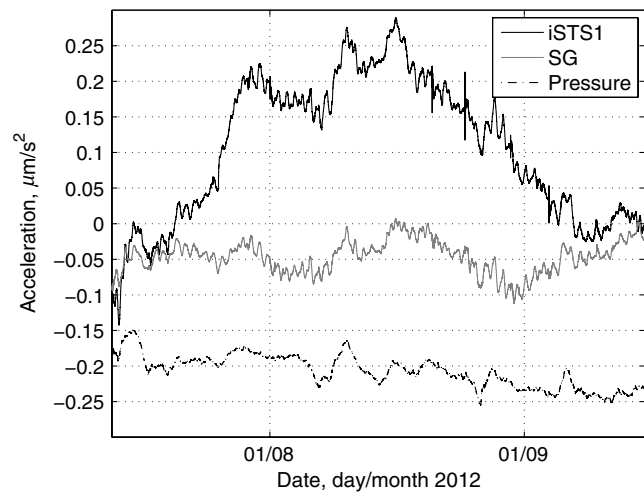


Figure 6. An example of correlations between barometric pressure changes and observed acceleration. The iSTS1 and SG graphs are plotted in the units shown on the vertical axis, and the pressure signal has been scaled by the value given in the text.

the frequency-by-frequency values are plotted to produce the minimum noise spectra. This procedure yields a robust estimate of the noise floor and is consistent with the procedure adopted by Berger *et al.* (2004) to determine the globally averaged GSN noise spectra.

In the frequency band between 2 and 8 mHz, we can see that the iSTS1 is somewhat noisier than the others but that at higher frequency noise levels are similar.

Normal Modes

We examined the records from the magnitude 9.0 Tohoku earthquake of 11 March 2011 to compare the spectra in the normal mode band during a 6-day interval starting 18.5 hr after the earthquake. We measured the ratios of the peak amplitudes of the 14 lowest-frequency modes, as observed on the four instruments (Fig. 9). The mean values of these observed ratios are

$$\begin{aligned} \text{SG/iSTS1} &= 0.998 \pm 0.029, \\ \text{SG/STS1} &= 1.027 \pm 0.009, \quad \text{and} \\ \text{SG/STS2} &= 1.000 \pm 0.06, \end{aligned}$$

which are in agreement with the M2 values.

Nonlinearities

A feedback seismometer uses analog signal processing and force feedback to minimize the effects of any suspension nonlinearity (because the mass does not move very far). The output linearity and dynamic range are then set by the analog feedback electronics and the forcer. The optical seismometer, in contrast, must use digital signal processing to suppress the nonlinearities of the mechanical suspension, so the output linearity is determined by the accuracy of the model and the precision of the digital processing.

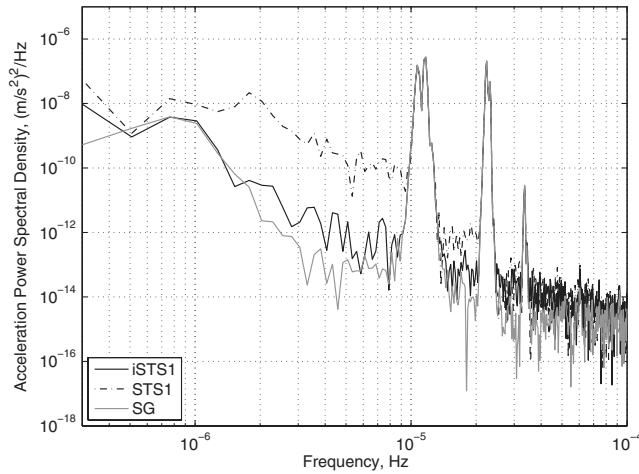


Figure 7. Spectra from three sensors around the tidal bands. The time series have been corrected for a pressure effect.

The coefficients c_1 and c_2 in equation (1) can be estimated either by testing on a shake table or by maximizing the correlation coefficient between an already linearized seismometer, say an STS1 or STS2, and the optical seismometer for a large signal.

The 11 March 2011 Tohoku, Japan, Earthquake

For the iSTS1, we did not linearize with a shake table prior to deployment at BFO. Instead, we used observations of earthquakes that produced large mass displacements. For example, the M_w 9.0 Tohoku earthquake produced a peak mass motion on the iSTS1 of about 0.45 mm (the peak ground velocity observed was 2.6×10^{-3} m/s $^{-1}$ and the peak ground acceleration was 1×10^{-3} m/s $^{-2}$). Both the SG and STS1 instruments were driven off the scale. On-scale recording, however, from the collocated STS2 was obtained for comparison. Figure 10 shows the records in which the iSTS1 data have been passed through a time-domain filter to match the reported response of the STS2. Performing a linear fit between these two records leaves only a residual variance of 6.5×10^{-4} of the original signal variance. Nonetheless, in the top panel of Figure 10, one can see a small signal in the trace of the residual. In the center panel, we emphasize this residual signal by low passing the record through a second-order Butterworth filter with a corner at 1200 s. We note that the largest nonlinearities occur for the P waves and for the crustal Rayleigh waves ($T = 25$ s) but not for the S waves or the mantle waves ($T = 250$ s), even though these phases constitute the largest signal in the low-pass filtered traces.

The values $c_1 = -0.01$ s $^{-2}$ and $c_2 = 69.5$ m $^{-1}$ /s $^{-2}$ were found to maximize the correlation coefficient between the STS2- and the iSTS1-derived velocity; the result with these values used in equation (2) is shown in the lowest panel of Figure 10.

The 20 May 2012 Mirandola, Italy, Earthquake

To see if these nonlinear coefficients change with time or frequency content, we examined the records of a moderate

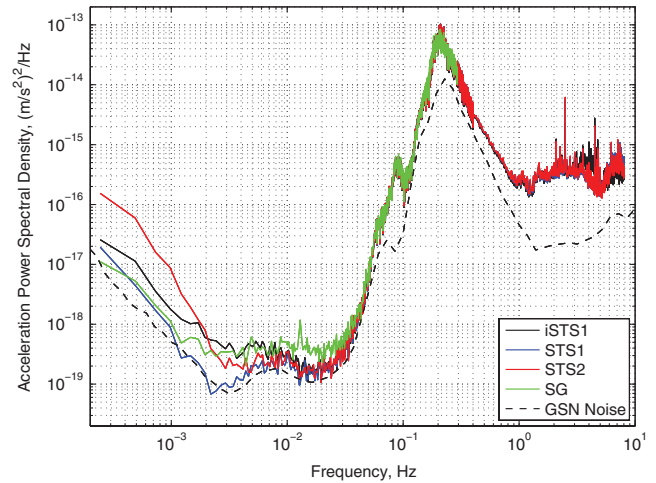


Figure 8. The spectra are estimated from pressure-corrected observations at sample rates of 1 sample per second for the long periods and 20 samples per second for the shorter periods. Each time series is divided into 16,384-sample 50% overlapping segments and then the spectra estimated with a 4096-sample Hanning window with 50% overlap. Finally, we plot the third percentile estimates at each frequency band. The bandwidth for these estimates is 2.385×10^{-5} Hz for frequencies less than 0.4 Hz and 4.77×10^{-3} Hz for higher frequencies. We limit the SG analysis frequencies lower than 0.33 Hz. Similar analyses from other epochs will give slightly different results.

regional event, which occurred over a year later. On 20 May 2012, there was an M 6.0 earthquake near Mirandola, Italy, approximately 440 km to the southeast of BFO. This earthquake produced peak-to-peak mass displacements of the iSTS1 of just over 1 mm, the largest yet recorded.

Using the parameters determined for the Tohoku earthquake produced the results shown in Figure 11. The iSTS1 fits the STS2 better than it fits the STS1, most likely because the STS2 was used to linearize the iSTS1 in the first place.

Conclusions

The goals of this work were to compare disparate vertical seismometers operating at the same site. This allowed us to check their calibrations with respect to one another in different frequency bands and provided an important check on the instruments' published frequency responses and gains. In addition, we were able to compare noise floors of the instruments at different frequencies. The BFO provides a unique setting, combining both a very stable thermal (and otherwise) environment, very low background seismic noise, and a diverse suite of instruments, making these comparisons possible.

Our first conclusion is that the calibrations of the instruments studied here, which include an optical seismometer (iSTS1), two conventional seismometers (an STS1 and an STS2), and a SG, agree well at the 1% level across a wide range of frequencies. However, one apparently cannot count on calibrations being stable to a higher precision than this because the comparisons had disagreements in some cases

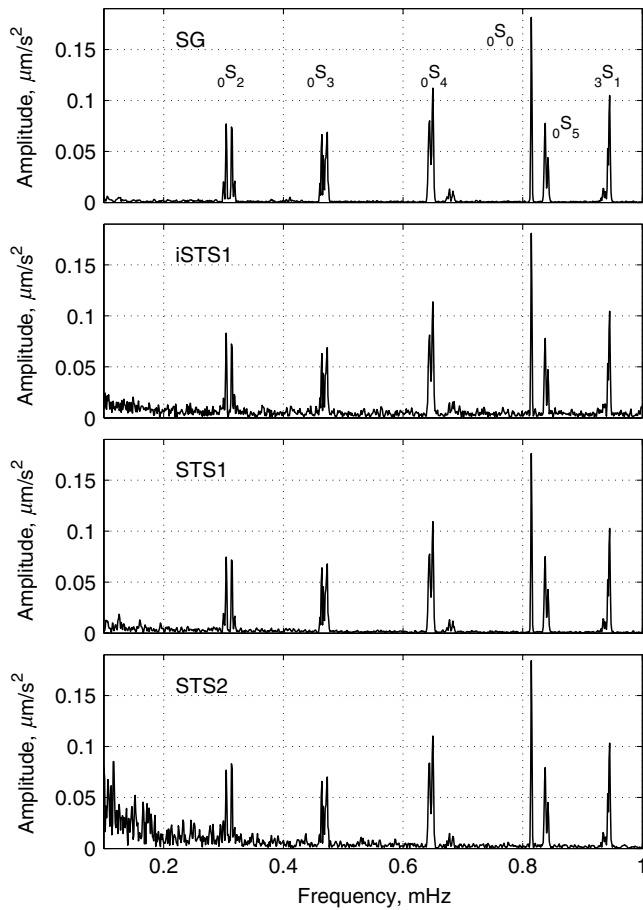


Figure 9. Spectra showing the lowest-order spheroidal multiplets as recorded starting 18.5 hr after the event and continuing for 272 hr. Coriolis splitting is clearly visible for the fundamental spheroidal modes. Barometric correction was applied to all of these spectra, however it only improved the signal to noise for the SG, which has the lowest noise in this band (Zürn and Widmer, 1995).

by several tenths of one percent and slightly exceeding 1% in some cases.

A key motivation for this research was to evaluate the performance of an optical seismometer. Our comparison of the iSTS1 to the SG and the standard STS1 and STS2 seismometers shows that the optical seismometer can provide data of nearly equal quality over a bandwidth spanning that of the other instruments, from a few microhertz to greater than 10 Hz; the optical seismometer has a larger dynamic range than either the STS1 or the SG. The coefficients of both the linear and nonlinear responses of the iSTS1 are shown to be constant at least over the epoch studied. The optical seismometer appears to provide a single sensor that is comparable to the best sensors in the noise floor across the entire range of frequencies studied (subtidal to seismic) and has a wider dynamic range than conventional seismometers. Its nonlinearity for very large or very close earthquakes can be modeled and corrected.

Although the performance of the optical seismometer is promising, challenges remain to make it practical. Digital signal processing is required to remove nonlinearities from

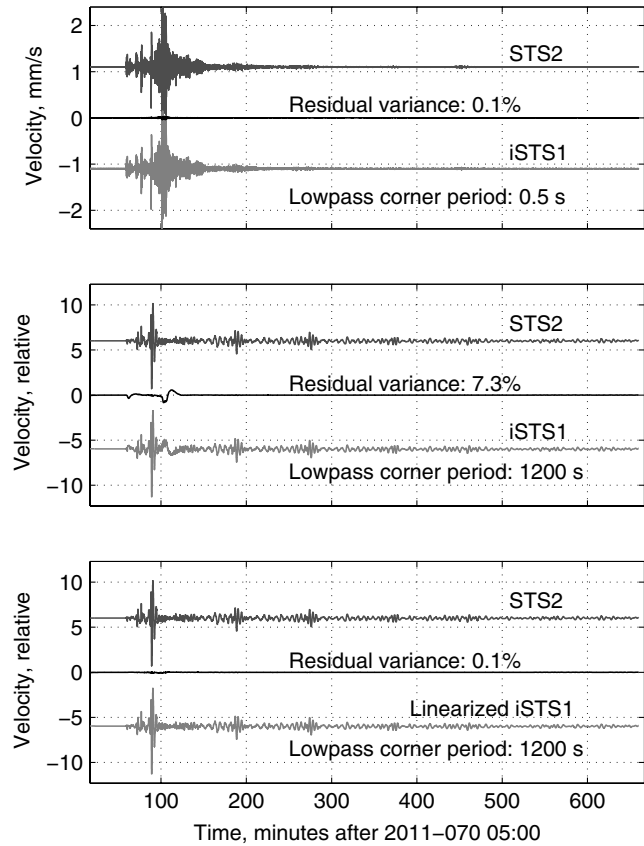


Figure 10. The upper plot shows the data at nearly full bandwidth, and the nonlinearity is not apparent. However, after low-pass filtering, a residual indicates the iSTS1 has a slight nonlinearity (middle plot). Fitting two coefficients in equation (1) produces the linearized result in the bottom plot. Because the data are low-pass filtered well below the passband of the STS2, the vertical scale is only relative.

large events. The optical system already includes a digital signal processor to extract the displacement from the interferometer fringe signals, and we have experimented with converting the mass displacement to ground velocity with the same processor. We expect it will be possible to add the nonlinear terms to the real-time processing software. This will require characterizing the suspension in the lab, knowing how the coefficients vary with position, then knowing the absolute position of the mass after installation in the field and having confidence that the lab calibrations remain valid in the field. This is made slightly more complicated by the fact that the optical displacement transducer is not absolute (it does not retain its zero level after an interruption). We have initial indications that the stabilities of the suspension coefficients are good, and we have noted that the drift in the mass position proceeds at only 15 μm per year, suggesting that once calibrated, frequent recalibrations would not be required. However, some work remains to confirm this on many examples of the same suspension design. This, and further improvements to lower the noise in the normal mode band so that it matches that of the STS1, are areas of ongoing research.

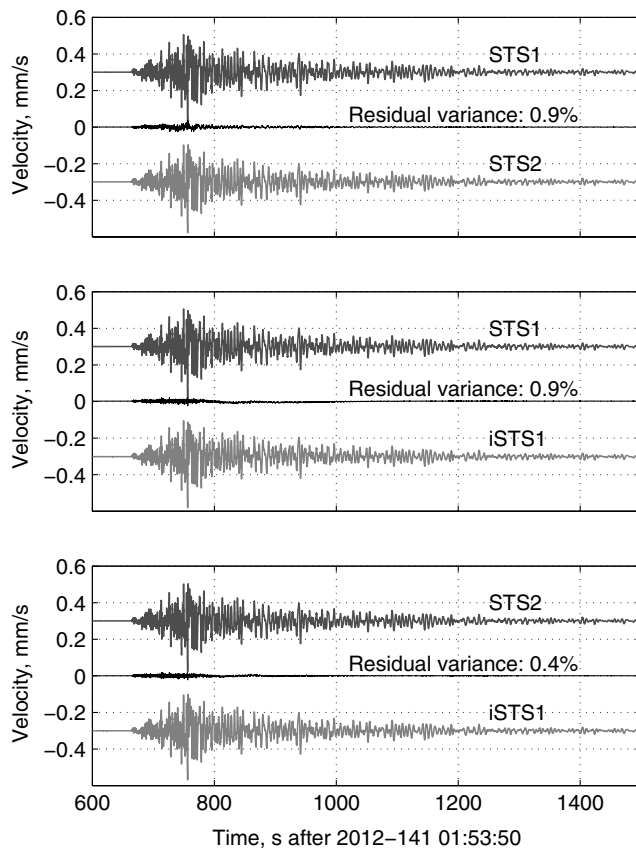


Figure 11. Nonlinear processing of iSTS1 record in comparison with both STS1 and STS2 records.

Data and Resources

Data from most of the instruments described here are currently available from the Incorporated Research Institutions for Seismology Data Management Center (IRIS DMC); however, many records had not yet been deposited there during the times analyzed in this work. Consequently, the data are available by requests to the authors. Information on the Black Forest Observatory may be found at <http://www.bfo.geophys.uni-stuttgart.de/> (last accessed June 2014). A. Grinsted's 2008 Tidal Fitting Toolbox (<http://www.mathworks.com/matlabcentral/fileexchange/19099-tidal-fitting-toolbox>; last accessed July 2014) was used for parts of the analysis.

Acknowledgments

The authors are grateful for financial support from the National Science Foundation (Award Numbers EAR0732418 and EAR0154050), the Incorporated Research Institutions for Seismology via cooperative agreement EAR-1063471, Scripps Institution of Oceanography, and the Green Foundation for Earth Sciences. We thank Erhard Wielandt for advice on the instrument design and on the data processing, William Hatfield (Institute of Geophysics and Planetary Physics) for painstakingly editing over a year of 1-sample-per-second data to remove artifacts, Peter Duffner (Black Forest Observatory [BFO]) for maintenance of the instruments used in the study, Thomas Forbriger (BFO) for help with the instrument calibrations, and the anonymous reviewers.

References

- Agnew, D. C. (1996). *SPOTL: Some Programs for Ocean-Tide Loading*, SIO Reference Series 96-98, Scripps Institution of Oceanography, La Jolla, California.
- Berger, J., P. Davis, and G. Ekström (2004). Ambient Earth noise: A survey of the Global Seismographic Network, *J. Geophys. Res.* **109**, no. B11307, doi: [10.1029/2004JB003408](https://doi.org/10.1029/2004JB003408).
- Davis, P., and J. Berger (2007). Calibration of the Global Seismographic Network using tides, *Seismol. Res. Lett.* **78**, 454–459.
- Fels, J.-F., and J. Berger (1994). Parametric analysis and calibration of the STS-1 seismometer of the IRIS/IDA seismographic network, *Bull. Seismol. Soc. Am.* **84**, 1580–1592.
- Goodkind, J. M. (1999). The superconducting gravimeter, *Rev. Sci. Instrum.* **70**, 4131, doi: [10.1063/1.1150092](https://doi.org/10.1063/1.1150092).
- Heck, A. (2014). Bestimmung des Frequenzgangs des Supraleitenden Gravimeters SG056, *Bachelor Thesis*, Institute of Geophysics, KIT Karlsruhe, Germany (in German).
- Rosat, S., and J. Hinderer (2011). Noise levels of superconducting gravimeters: Updated comparison and time stability, *Bull. Seismol. Soc. Am.* **101**, 1233–1241.
- Van Camp, M., H.-G. Wenzel, P. Schott, P. Vauterin, and O. Francis (2000). Accurate transfer function determination for superconducting gravimeters, *Geophys. Res. Lett.* **27**, 37–40.
- Widmer-Schmidrig, R. (2003). What can superconducting gravimeters contribute to normal-mode seismology? *Bull. Seismol. Soc. Am.* **93**, 1370–1380.
- Widmer-Schmidrig, R., W. Zürn, P. Duffner, and Th. Forbriger (2012). The dual-sphere superconducting gravimeter at BFO—Long-period signals and instrumental drift, poster presented at the *Annual Meeting of the German Geophysical Society (DGG)*, Hamburg, Germany, http://www.geophys.uni-stuttgart.de/~widmer/SG056-Poster_DGG_2012.pdf (last accessed July 2014).
- Wielandt, E. (2012). Seismic sensors and their calibration, in *New Manual of Seismological Observatory Practice 2 (NMSOP-2)*, P. Bormann (Editor), <http://www.iaspei.org/projects/NMSOP.html>, doi: [10.2312/GFZ.NMSOP-2_ch5](https://doi.org/10.2312/GFZ.NMSOP-2_ch5) (last accessed July 2014).
- Wielandt, E., and G. Streckeisen (1982). The leaf-spring seismometer: Design and performance, *Bull. Seismol. Soc. Am.* **72**, 2349–2367.
- Zumberge, M. A., J. Berger, M. A. Dziedziuch, and R. L. Parker (2004). Resolving quadrature fringes in real time, *Appl. Opt.* **43**, 771–775.
- Zumberge, M. A., J. Berger, J. Otero, and E. Wielandt (2010). An optical seismometer without force feedback, *Bull. Seismol. Soc. Am.* **100**, 598–605, doi: [10.1785/0120090136](https://doi.org/10.1785/0120090136).
- Zürn, W., and R. Widmer (1995). On noise reduction in vertical seismic records below 2 mHz using local barometric pressure, *Geophys. Res. Lett.* **22**, 3537–3540.

Institute of Geophysics and Planetary Physics
Scripps Institution of Oceanography
University of California, San Diego
La Jolla, California 92093-0225
jberger@ucsd.edu
pdavis@ucsd.edu
zumberge@ucsd.edu
(J.B., P.D., M.Z.)

Black Forrest Observatory
Heubach 206
77709 Wolfach
Germany
widmer@geophys.uni-stuttgart.de
(R.W.-S.)

Manuscript received 24 February 2014;
Published Online 26 August 2014